

Ventricular activation during sympathetic imbalance and its computational reconstruction

MARTYN P. NASH,¹ JUDITH M. THORNTON,¹ CLAIRE E. SEARS,²
ANTHONY VARGHESE,³ MARK O'NEILL,¹ AND DAVID J. PATERSON¹

¹University Laboratory of Physiology, Oxford OX1 3PT; and ²Department of Cardiovascular Medicine, John Radcliffe Hospital, Oxford OX3 9DU, United Kingdom; and ³Institute for Mathematics and its Applications, University of Minnesota, Minneapolis, Minnesota 55455

Received 20 June 2000; accepted in final form 11 August 2000

Nash, Martyn P., Judith M. Thornton, Claire E. Sears, Anthony Varghese, Mark O'Neill, and David J. Paterson. Ventricular activation during sympathetic imbalance and its computational reconstruction. *J Appl Physiol* 90: 287–298, 2001.—We characterized the epicardial activation sequence during a norepinephrine (NE)-induced ventricular arrhythmia in anesthetized pigs and studied factors that modulated it. Subepicardial NE infusion caused the QRS complex to invert within a single beat ($n = 35$ animals, 101 observations), and the earliest epicardial activation consistently shifted to the randomly located infusion site ($n = 14$). This preceded right atrial activation, whereas the total ventricular epicardial activation time increased from 20 ± 4 to 50 ± 9 ms ($P < 0.01$). These events were accompanied by a ventricular tachycardia and a drop in left ventricular pressure, which were fully reversed after the infusion was stopped. Epicardial pacing at the infusion site mimicked all electrical and hemodynamic changes induced by NE. The arrhythmia was prevented by propranolol and abolished by cardiac sympathetic or vagal nerve stimulation. Focal automaticity was computationally reconstructed using a two-dimensional sheet of 256×256 resistively coupled ventricular cells, where calcium handling was abnormally high in the central region. We conclude that adrenergic stimulation to a small region of the ventricle elicits triggered automaticity and that computational reconstruction implicates calcium overload. Interventions that reduce spatial inhomogeneities of intracellular calcium may prevent this type of arrhythmia.

catecholamines; cardiac mapping; porcine heart; ventricular arrhythmia

IT IS WELL ESTABLISHED THAT cardiac sympathetic imbalance can lead to ventricular arrhythmias, although the underlying cellular electrophysiological mechanisms are not fully understood. Phase 4 depolarization (abnormal automaticity) and afterdepolarizations (triggered automaticity) (22) have been implicated because both can be provoked by catecholamines (8, 27) or exercise (8) and prevented or terminated by β -adrenergic blockade (8) and acetylcholine (27), all of which modulate the levels of intracellular calcium in ventricular myocytes. Calcium-channel antagonists also prevent triggered automaticity (8, 27), whereas they are

ineffective in terminating abnormal automaticity (27). Previous studies (18, 19) have shown that, in the in vivo nonischemic pig heart, a localized subepicardial infusion of norepinephrine (NE), the permeant cyclic-AMP analog dibutyryl-cAMP, or inhibitors of cyclic nucleotide phosphodiesterase were effective in causing a sustained ventricular arrhythmia, resulting in depressed hemodynamics. In the clinical situation, high-adrenergic tone is known to occur around regions of ischemia (11) or during right ventricular (RV) outflow tract dysfunction (16), both of which may facilitate spontaneous activity in the ventricular myocardium (10).

Our aims were threefold: 1) to test whether the hemodynamic changes were a direct consequence of the formation of a new pacemaker at the NE infusion site; 2) to examine whether changing global cardiac autonomic input, through stimulation of the cardiac sympathetic or vagal nerves, modulated the electrical activation sequence during the arrhythmia and whether electrical pacing at the infusion site mimicked the pattern of activation caused by the infusion of NE; and 3) to elucidate the electrophysiological basis underlying this arrhythmia, we attempted to reconstruct it in two dimensions using a network model of 256×256 resistively coupled ventricular cells, for which the central region had high-adrenergic tone. Some of the results have been communicated in abstract form (12, 13).

MATERIALS AND METHODS

The investigation conforms to the “Guide for the Care and Use of Laboratory Animals” published by the National Institutes of Health [DHEW publication no. (NIH) 85–23, revised 1996, Office of Science and Health Reports, DRR/NIH, Bethesda, MD 20205] and under a British Home Office Project License (no. PPL 30/1133).

Anesthesia

Thirty-five domestic pigs of either sex [mean weight, 24 ± 5 (SD) kg] were premedicated with azaperone (5 mg/kg im;

Address for reprint requests and other correspondence: M. P. Nash, Univ. Laboratory of Physiology, Parks Road, Oxford OX1 3PT, UK (E-mail: martyn.nash@physiol.ox.ac.uk).

The costs of publication of this article were defrayed in part by the payment of page charges. The article must therefore be hereby marked “advertisement” in accordance with 18 U.S.C. Section 1734 solely to indicate this fact.

Stresnil, Janssen), and a surgical plane of anesthesia was induced with 2–3% halothane (Fluothane, ICI) in 100% oxygen via an Ayre's T piece with a mask and bag. After the surgery, halothane was replaced with a bolus infusion of α -chloralose (100 mg/kg iv; Sigma Chemical) and repeated approximately every 2 h as required. Stainless steel needle electrodes were then inserted subcutaneously into each limb and into the chest wall to monitor the electrocardiograph (ECG).

Surgery and Instrumentation

A tracheotomy was performed, and a cuffed endotracheal tube (9 mm, Vygon) was introduced ~80 mm into the trachea. The cuff was inflated to provide an airtight seal. Fluid-filled catheters (Portex) were inserted into two femoral arteries and one femoral vein for sampling of arterial blood, monitoring of arterial blood pressure (ABP), and intravenous infusion of anesthetic and fluids, respectively. Artificial ventilation (Oxford Mark II ventilator, Penlon) was used to maintain arterial carbon dioxide tension between 35 and 45 Torr by adjusting tidal volume and frequency as required. Animals were ventilated with a hyperoxic gas mixture throughout the experiment. A midline thoracotomy was performed, and the chest was retracted laterally. After incision of the pericardium, the heart was suspended in a pericardial cradle. For all experiments, the cranial projections of the vagi were cut.

In the first group of experiments (*group A*, $n = 21$), a catheter (Wallace Y-can, 19 gauge) was inserted into the left ventricle (LV) via the apical dimple and secured. The cranial projections of the cardiac sympathetic nerves were ligated and cut. Communicating branches to the thoracic sympathetic chain were also cut.

In the second group of animals (*group B*, $n = 14$), a Millar catheter (Mikro-Tip, TC-510 control unit; Millar Instruments, Houston, TX) pressure sensor was inserted into the LV via the apical dimple. An elasticized sock containing 127 unipolar stainless steel electrodes (Biomedical Instruments Designers, Montreal, Quebec) was slipped over the ventricles. In addition, one custom-built silver electrode was attached to the right atrium with the use of continuous suction.

Intensive Care

After completion of surgery, at least 1 h elapsed before experiments were begun. The thoracic cavity was covered by plastic film to reduce cooling. Core body temperature was measured by a rectal thermistor and maintained at $38 \pm 1^\circ\text{C}$ by heating lamps beneath the operating table. Fluid was replaced by an intravenous sterile saline drip (~100 ml/h). Arterial blood samples (0.3 ml) were regularly withdrawn into preheparinized syringes and analyzed for pH, blood gases, and electrolytes (Na^+ , K^+ , Ca^{2+}) (Radiometer ABL505, Copenhagen, Denmark). For all animals ($n = 35$), mean values for arterial pH, arterial CO_2 tension, and arterial O_2 tension were 7.44 ± 0.07 (SD), 41 ± 6 Torr, and 319 ± 86 Torr, respectively. Respiratory acidosis was corrected by adjusting the ventilator. Metabolic acidosis was corrected by intravenous infusion of 4.2% sodium bicarbonate solution as required.

Hemodynamic Measurements

ABP was measured by using a saline-filled pressure transducer (Sensonor 840) calibrated in the midaxillary line. For *group A*, left ventricular pressure (LVP) was also measured in this way, and, for *group B*, LVP was measured directly by

using the Millar catheter. All signals were recorded onto a penwriter (MT8P, Lectromed). The analog inputs were passed to a real-time data-acquisition system (MP 100, Biopac Systems) employing Acqknowledge 3.0 software for the Macintosh (Macintosh Quadra 950). Heart rate (HR) and the rate of change of LVP (LVdP/dt) were computed using this software.

Epicardial Electropotential Mapping

For the experiments in *group B*, 63 of the sock electrodes and the right atrial electrode were connected to a 64-channel Unemap cardiac mapping system (Uniservices, Auckland, New Zealand). The selected sock electrodes spanned the whole of the ventricular epicardium, with an interelectrode spacing of ~15 mm. The animal and all cable shields were earthed to the system ground (computer earth potential). Unipolar epicardial electropotentials (referred to the system ground) were continuously sampled at 900 Hz with a rolling buffer of 8 s and could be digitally stored for subsequent analysis. During three of these experiments, two-dimensional echocardiography (HP SONOS 5500) was used to estimate LV ejection fraction.

Protocols

In all animals ($n = 35$), ventricular arrhythmias were induced by regional subepicardial infusions of NE bitartrate (10 $\mu\text{mol/l}$ in 0.9% saline, 150 $\mu\text{l/min}$). The concentration and rate of infusion were chosen because they elicited reproducible arrhythmias within 1–5 min after the onset of the infusion. Infusion was through a 25-gauge hypodermic needle to which was attached a 3FG polyvinyl chloride catheter (~150 mm long) and a three-way tap. The needle was inserted 1–5 mm at randomly selected locations throughout the ventricular subepicardium. Solutions were infused by using a three-syringe microinjection pump (CMA/100). In cases in which subepicardial infusion of NE did not elicit a ventricular arrhythmia within 5 min (~20% of infusions), the needle was removed, and infusion was begun in another part of the ventricle. Susceptibility to the arrhythmia did not depend on the choice of infusion site.

Group A ($n = 21$). The vehicle (saline) was infused (150 $\mu\text{l/min}$) subepicardially in all animals for ~10–15 min.

To test whether the arrhythmia was due to β -adrenergic stimulation alone, propranolol (0.1–0.25 mg/kg iv; Inderal, ICI) was administered during the NE-induced ventricular arrhythmia ($n = 8$). The specific β -agonist isoproterenol (1 $\mu\text{mol/l}$, 150 $\mu\text{l/min}$, $n = 2$) or the α -agonist phenylephrine (1 and 10 $\mu\text{mol/l}$, 150 $\mu\text{l/min}$, $n = 2$) was also infused subepicardially in the absence of β -blockade.

To test whether the arrhythmia could be modulated by global autonomic input, cardiac sympathetic nerve stimulation (5 Hz, 5 V, 3-ms width, 30-s duration; caudal limb of the right ansa subclavia, $n = 6$) or vagal nerve stimulation (10 Hz, 10 V, 3-ms width, 30-s duration; left vagus, $n = 2$; right vagus, $n = 4$) was undertaken during the NE-induced ventricular arrhythmia. Each period of stimulation lasted for 30 s and was followed by a recovery period, while the infusion of NE was maintained. Pre- and postarrhythmia stimulations were also performed to test the stability of the nerves. In addition, NE was infused intravenously (1 $\mu\text{g}\cdot\text{kg}^{-1}\cdot\text{min}^{-1}$ for 1 min) during stable arrhythmias ($n = 3$). Control intravenous infusions of NE were also performed before subepicardial NE infusion.

Group B ($n = 14$). Ventricular electropotential mapping was performed for control, NE-induced ventricular arrhyth-

mia, and recovery states. In addition, a single electrode was used to detect right atrial activation ($n = 10$).

A custom-built roving bipolar electrode was used to pace hearts (0.5–1.5 V, 2-ms width, 30-s duration, $n = 3$) at the same site in which NE had previously been infused. The pacing needle was inserted ~ 2 mm subepicardially, and the pacing rate was matched to the HR observed during the previous NE-induced arrhythmia.

Epicardial surface ($n = 2$) or transesophageal ($n = 1$) echocardiography was used to estimate LV ejection fraction during the ventricular arrhythmias.

Electropotential Signal Analysis

With reference to Fig. 1, epicardial electropotential signal analysis was performed as follows. After epicardial signal acquisition using the elasticized electrode sock (Fig. 1A), the electropotentials for a single heart cycle were identified from the 8 s of recorded data, as shown in Fig. 1B. The most negative electropotential slope was computed for each signal (Fig. 1C), and this was chosen to mark the instant at which the associated sock electrode detected excitation of its adjacent portion of epicardium. An event marker was used to identify the time of excitation for each signal.

The set of event markers was then used to order the signals, such that the signal that detected earliest activation was listed first (Fig. 1C). For this earliest signal, the marker

time was referred to as the datum (red dashed line in Fig. 1C). Activation times were then computed for all other signals by taking the difference between their marker times and the datum.

Two-dimensional Activation Maps

From the known topographical organization of the sock electrodes, estimated epicardial electrode locations were plotted by using the two-dimensional Hammer projection (20), for which the LV and RV free walls constitute the central and lateral portions, respectively (see Fig. 1D). The left anterior and posterior descending coronary arteries were superimposed for anatomic clarity. Nodal activation times were computed from the set of spatially arranged electrode activation times using a two-dimensional finite element-fitting technique, which incorporated linear least squares (6). Red portions of this smoothly continuous two-dimensional activation map highlight regions of earliest epicardial excitation, whereas blue denotes regions of latest epicardial excitation. The spatial resolution of the electrodes was considered sufficient during control and arrhythmic states, because doubling the electrode density (i.e., halving the interelectrode spacing) over one-half of the epicardial surface produced a similar two-dimensional activation pattern and range of times for that region (not shown).

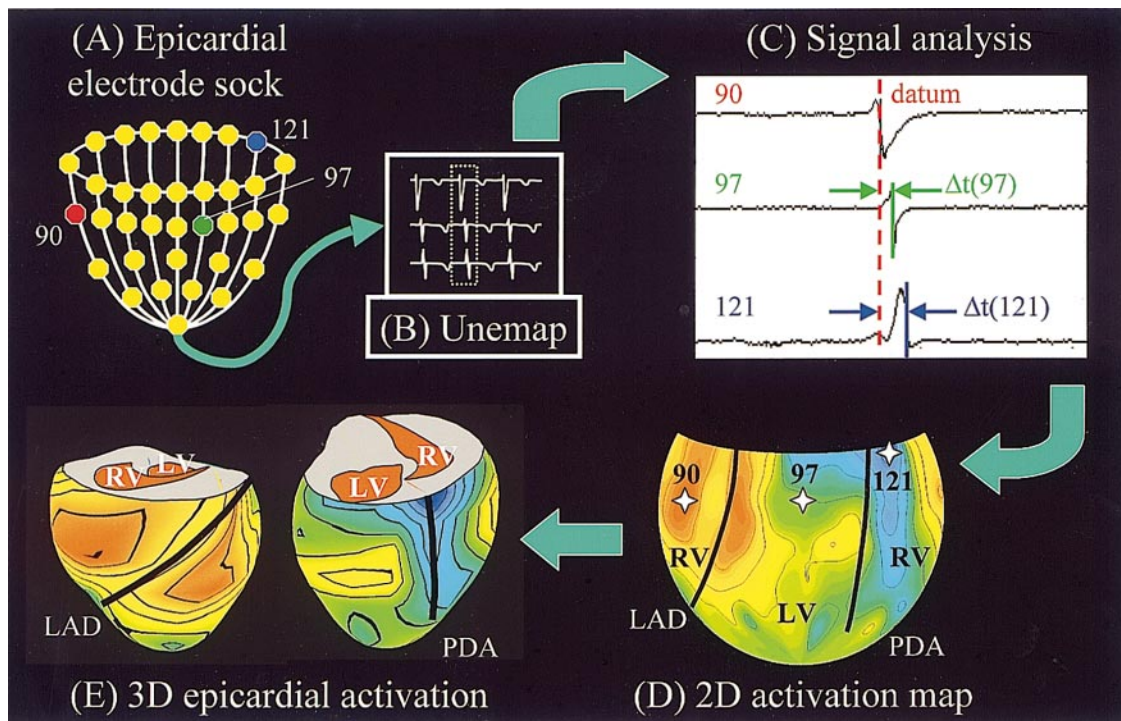


Fig. 1. Schematic representation of cardiac electropotential mapping and signal analysis. Epicardial signals were recorded by using an elasticized sock with 63 epicardial electrodes (A) connected to a cardiac mapping system (B). C: a single heart cycle was identified, and the epicardial activation time for each electrode was determined by using the most negative electropotential slope. Δt , Time difference. D: an epicardial activation map was fitted to the electrode activation times and displayed by using the Hammer projection. This 2-dimensional (2D) topography represents the ventricular epicardial surface, where the left ventricle (LV) makes up the central portion of the projection, the right ventricle (RV) comprises the border regions, but the apex is retained as a single point. E: the activation time field was also fitted to the epicardial surface of an anatomically accurate 3-dimensional (3D) mathematical model of the ventricles, for which anterior (left) and posterior (right) views are illustrated and contours of simultaneous epicardial activation have been superimposed. LAD and PDA (thick lines), left anterior and posterior descending coronary arteries, respectively.

Epicardial Activation Sequence Rendered in Three Dimensions

A further technique was developed to produce epicardial activation maps with anatomic realism. The epicardial activation sequence was reconstructed by fitting a scalar field of activation times onto the epicardial surface of an anatomically accurate mathematical model of the canine ventricles (14) rendered in three dimensions, as shown in Fig. 1E. The estimated three-dimensional locations of the electrodes were projected onto the epicardial surface of the anatomic model, and the epicardial activation time field was approximated by using linear interpolation of a set of parameters defined at spatial locations that coincided with the finite element nodes used to define the geometry. As for the two-dimensional activation map, nodal epicardial activation times were computed by using a standard finite element-fitting technique.

Computer Modeling

Abnormal intracellular calcium handling has been implicated in the onset of this arrhythmia (18). In an attempt to simulate this, we modified a recent model of the electrical

activity in ventricular myocytes (15) to include effects of NE on cell membrane properties. The effect of NE was modeled by using a fivefold elevation in the conductances of the L-type calcium channel of the cell sarcolemmal membrane (from 0.25 to 1.25 $\mu\text{A}\cdot\text{l}\cdot\text{mmol}^{-1}$) and the sarcoplasmic reticulum (SR) calcium-ATPase uptake pump (from 1 to 5 $\text{mmol}\cdot\text{l}^{-1}\cdot\text{s}^{-1}$). This is consistent with changes in calcium currents due to isoproterenol that have been reported in the literature (1). Action potential propagation was studied by using a two-dimensional sheet of 256×256 cells isotropically interconnected via linear resistors to represent the intercellular gap junctions. To simulate the spatial decrease in NE concentration due to ligand diffusion and metabolism, the upregulation factor for the L-type and SR uptake calcium conductances was chosen to decrease according to a two-dimensional normal distribution with a variance of 60 cell lengths. In this way, conductance changes were negligible at a distance of 90 cell lengths from the center, consistent with the reported zone of increased cAMP levels surrounding intramyocardial NE infusion sites (18). Action potentials were initiated by stimulating one edge of the sheet at a rate of 1 Hz with a twice-threshold stimulus for 2 ms. A control

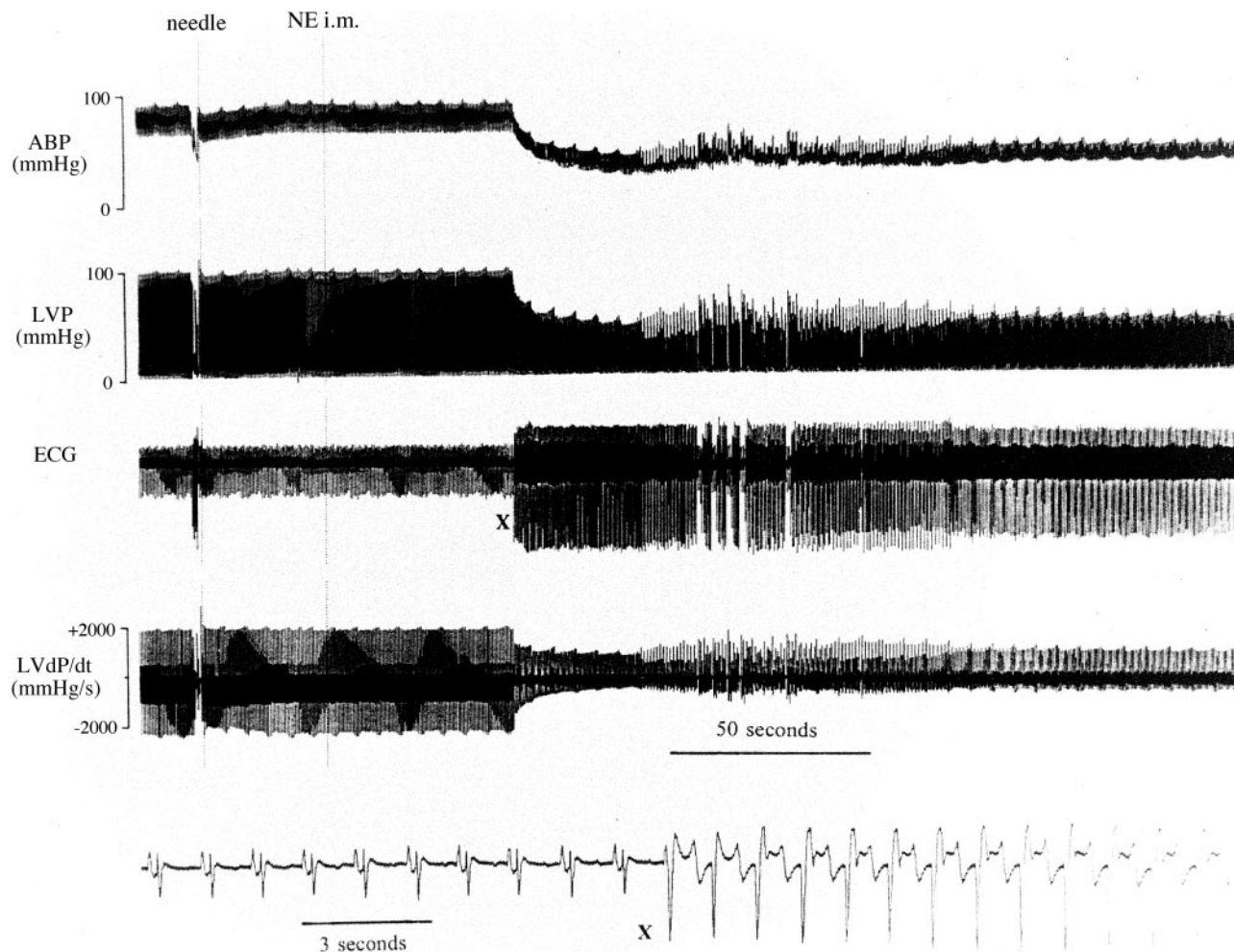


Fig. 2. Induction of a ventricular arrhythmia by subepicardial infusion ($150 \mu\text{l}/\text{min}$) of $10 \mu\text{mol}/\text{l}$ norepinephrine (NE). Needle, insertion point of needle; NE im, start of infusion. Traces are as follows (from the top down): arterial blood pressure (ABP), LV pressure (LVP), electrocardiograph (ECG), and rate of change of LVP (LVdP/dt). Bottom trace illustrates the ECG at the point marked X, but on an expanded time scale. Approximately 90 s after the NE infusion was begun, there was a dramatic change in the configuration of the ECG, which was accompanied by a marked hemodynamic depression.

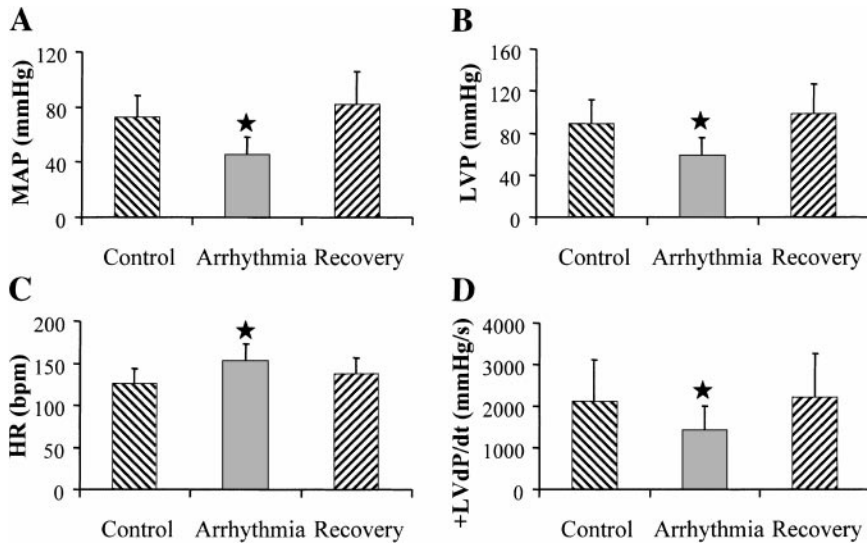


Fig. 3. Effect of subepicardial infusion ($150 \mu\text{l}/\text{min}$) of $10 \mu\text{mol/l}$ NE on hemodynamics for all experiments ($n = 35$ animals, 101 observations). Values correspond to those before infusion (control), the maximum hemodynamic depression during NE infusion (arrhythmia), and the values reached after termination of the arrhythmia (recovery). A: mean arterial blood pressure (MAP); B: maximum systolic LVP; C: heart rate (HR); D: maximum LVdP/dt ($+\text{LVdP}/\text{dt}$). bpm, Beats/min. \star Statistically significant ($P < 0.01$) changes in the hemodynamic variables compared with the control state.

simulation with normal intracellular calcium handling was undertaken for the same number of cycles. The ionic currents of a single-model myocyte were also investigated to elucidate a possible cellular mechanism for the NE-induced arrhythmia.

Cellular simulations were initially performed by using a Silicon Graphics Power Challenge XL (12 symmetric MIPS 90-MHz R8000 processors; 1-GB physical DRAM) and subsequently by using a Silicon Graphics Cray Origin2000 (84 symmetric MIPS 195-MHz R10000 processors; 21-GB physical DRAM; Silicon Graphics, Mountain View, CA). The parallel computations incorporated a variable-step, fourth-order, Runge-Kutta numerical integration method, as described previously (26).

Statistical Analysis

All data are expressed as means \pm SD. Mean arterial blood pressure (MAP), LVP, HR, LVdP/dt , and activation times for control, arrhythmic, and recovery states were compared by using a one-way analysis of variance with repeated measures. Post hoc comparisons were performed by using Dunnett's method, and statistical significance was accepted at $P < 0.05$.

RESULTS

NE-induced Ventricular Arrhythmia

Infusion of NE into the ventricular subepicardium elicited a reproducible ventricular arrhythmia on 101 separate occasions in 35 animals. Within 1–5 min after the start of the infusion, there was a marked change in the amplitude and direction of the QRS complex, which masked the P wave (Fig. 2). The abnormal electrical activity was accompanied by a ventricular tachycardia (control, 126 ± 18 beats/min; arrhythmia, 153 ± 20 beats/min; $P < 0.01$, $n = 35$) and a profound hemodynamic depression (see Figs. 2 and 3). Restoration of normal sinus rhythm and hemodynamic performance occurred within 10 min after the subepicardial infusion of NE was stopped. Recovery was accompanied by a small, transient overshoot of all hemodynamic variables (Fig. 3), which was significant compared with

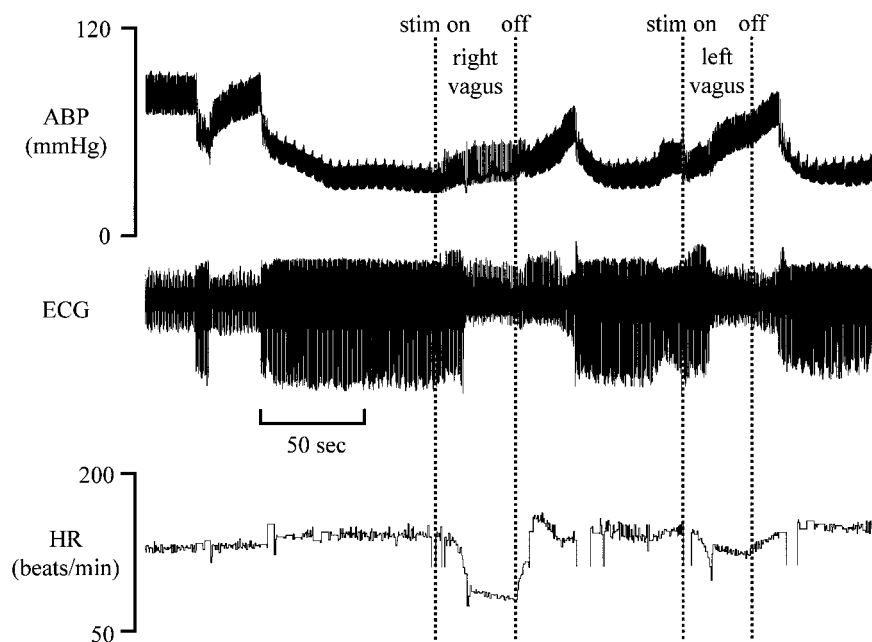
control ($P < 0.05$; $n = 35$). A subsequent ventricular arrhythmia could be established by using the same NE infusion site.

Sustained ventricular arrhythmia was also elicited by subepicardial infusion of the β -agonist isoproterenol ($n = 2$), but could not be provoked with subepicardial infusions of the α -agonist phenylephrine ($n = 2$) or the saline vehicle ($n = 21$), or by similar infusions of NE administered intravenously. After a stable arrhythmia was established, intravenous administration of a bolus of propranolol ($n = 8$) abolished it within ~ 2 min. After this, the hemodynamic performance quickly returned to its prearrhythmic state. It was not possible to elicit the arrhythmia in the β -blocked animal.

Sympathetic nerve stimulation. Stimulation of the right cardiac sympathetic nerve abolished the ventricular arrhythmia within 10.6 ± 7.5 s (17 observations in 6 animals). Sympathetic nerve stimulation caused the QRS complex to revert to its control form and the HR to increase by 90 ± 16 beats/min above the arrhythmic rate. No recurrence of the arrhythmia was seen during any 30-s period of sympathetic stimulation. However, the arrhythmia and hemodynamic depression were re-established 47 ± 16 s after stimulation was stopped. Infusion of NE ($1 \mu\text{g} \cdot \text{kg}^{-1} \cdot \text{min}^{-1}$ iv) for 1 min reversed the arrhythmia within 35 ± 21 s (5 observations in 3 animals). As observed during sympathetic stimulation, the QRS complex reverted, and all hemodynamic variables were elevated (HR increased by 42 ± 34 beats/min above the arrhythmic rate). Recurrence of the arrhythmia took place 30 ± 28 s after the infusion was stopped.

Vagal nerve stimulation. Stimulation of the left (5 observations in 2 animals) or right (13 observations in 4 animals) vagus nerves reversed the ventricular arrhythmia after 7.4 ± 4.9 s. Although control vagal stimulation reduced all hemodynamic variables, vagal stimulation during a NE-induced arrhythmia caused small increases in ABP, LVP, and LVdP/dt (see Fig. 4), whereas the HR decreased by 46 ± 11 beats/min after

Fig. 4. Effects of right and left cardiac vagal nerve stimulation [10 Hz, 10 V, 3-ms width, 30-s duration from stimulation (stim on)] during a subepicardial NE-induced ventricular arrhythmia. The sustained arrhythmia was elicited ~ 180 s after the onset of NE infusion (not shown). Traces are as follows (from top down): ABP, ECG, and HR. Both right and left vagal stimulation reversed the ECG inversion, but the arrhythmia recurred shortly after stimulation was stopped (stim off). The lack of recovery of the ABP during right vagal stimulation was likely due to the greater decrease in HR, compared with the effects of left vagal stimulation.



the termination of the arrhythmia. After the stimulation was stopped, hemodynamics continued to increase in the presence of normal electrical activity (Fig. 4) for 31 ± 9 s until the arrhythmia was reestablished.

Epicardial Electropotential Mapping

During the NE-induced arrhythmia for the *group B* experiments, right atrial activation followed the earliest ventricular epicardial activation (20 observations in 10 animals). Figure 5 illustrates the onset of one arrhythmia. The first two cycles show control conditions, in which right atrial excitation preceded ventricular activation. After the ventricular repolarization of the second cycle, a spontaneous ventricular depolarization was observed. Subsequently, earliest ventricular activation preceded right atrial activation on a one-to-one basis until after the NE infusion was stopped.

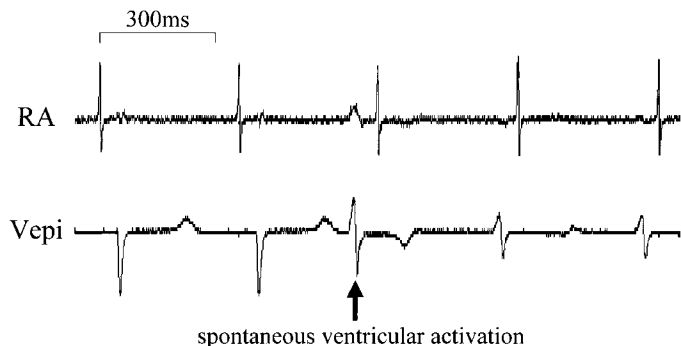


Fig. 5. Right atrial (RA) vs. ventricular epicardial (Vepi) electropotential recordings at the onset of a subepicardial NE-induced ventricular arrhythmia. Under control conditions (first 2 cycles), RA activation preceded Vepi activation. A spontaneous ventricular activation marks the onset of the arrhythmia, after which RA activation followed Vepi activation on a one-to-one basis.

Figure 6 illustrates epicardial activation maps during one experiment, for which a ventricular arrhythmia was elicited after ~ 90 s of NE infusion. Under control conditions, the earliest epicardial activation occurred near the equatorial region of the RV and the latest epicardial activation occurred in the postero-basal region. In this experiment, NE was infused near the apex of the posterior LV wall, and, during the ensuing arrhythmia, the location of earliest epicardial activation closely matched the NE infusion site. This change in the cardiac activation sequence caused the QRS complex to invert within a single beat and resulted in a marked depression of the ABP. Within 2 min of the stop of the NE infusion, the cardiac activation sequence, ECG, and hemodynamics were restored to their control states.

The events described above were observed consistently for all *group B* experiments (27 observations in 14 animals). The group data (see Fig. 7) showed that the total ventricular epicardial activation time (defined as the time taken for the wave of excitation to spread from earliest to latest epicardial activation sites) significantly increased from 20 ± 4 ms under control conditions to 50 ± 9 ms ($P < 0.01$, $n = 14$) during the NE-induced ventricular arrhythmia. During all 27 NE-induced arrhythmias, earliest epicardial activation was detected within one electrode spacing (~ 15 mm) of the needle site. The MAP significantly decreased from 62 ± 13 mmHg (control) to 43 ± 10 mmHg during the arrhythmia ($P < 0.01$, $n = 14$). The total ventricular epicardial activation time and MAP recovered to control values after the NE infusion was stopped.

Epicardial electrical stimulation. Ventricular epicardial pacing at the NE infusion site mimicked all electromechanical changes observed during the NE-induced ventricular arrhythmia. Figure 8 shows activation maps obtained during one experiment, for which

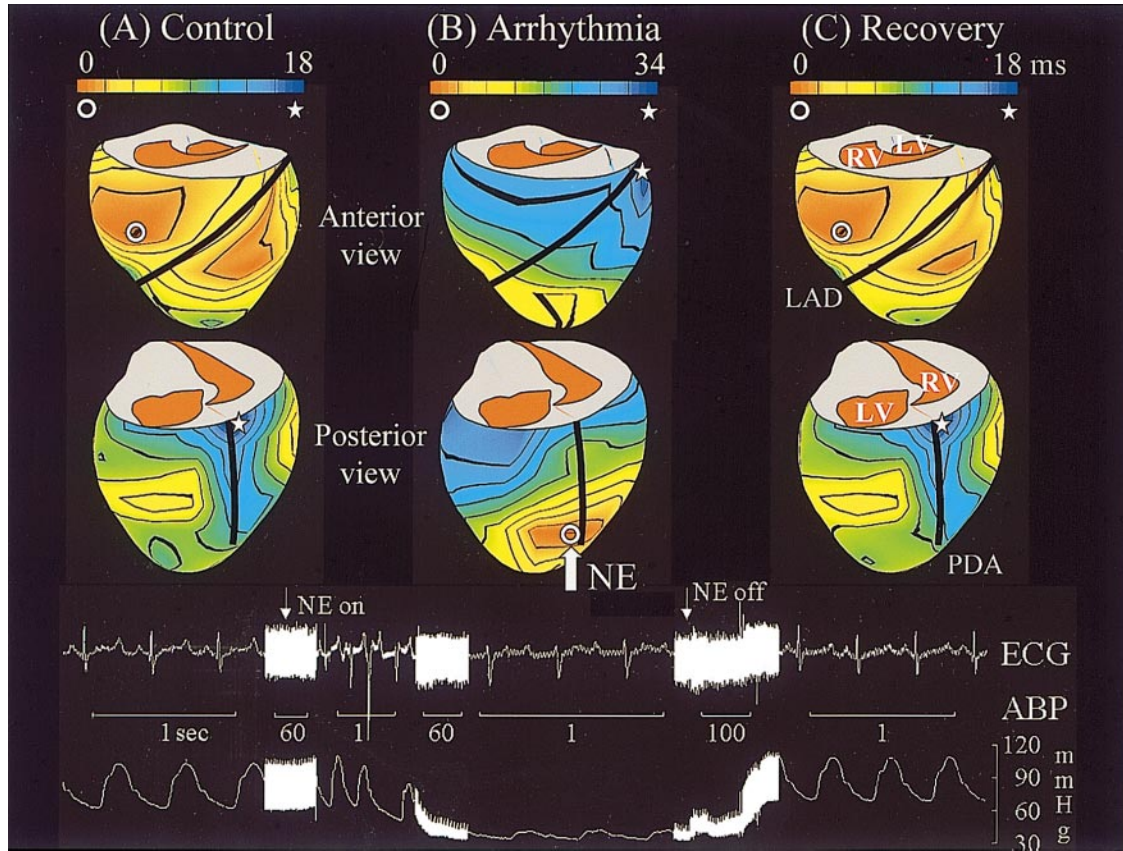


Fig. 6. Epicardial activation sequences superimposed on an anatomically accurate 3D mathematical model of the ventricles during normal sinus rhythm (A), NE-induced ventricular arrhythmia (B), and recovery (C). Earliest epicardial activation (o) shifted from the apical regions of the RV free wall during control conditions to the NE infusion site (thick white arrow) near the apex of the LV free wall during the arrhythmia. Latest epicardial activation (☆) occurred adjacent to the posterobasal portions of the interventricular septum under control conditions but moved to the posterobasal region of the LV free wall during the arrhythmia. At the onset of the arrhythmia, the QRS complex of the ECG inverted, and this was immediately followed by a dramatic decrease in the ABP. All changes were fully reversed after the infusion was stopped. Thick black lines denote the LAD and PDA coronary arteries.

NE was infused into a LV equatorial site. The subsequent arrhythmia resulted in an increase in the total ventricular epicardial activation time from 21 ms (control) to 49 ms. After a full recovery, the needle was withdrawn, and the epicardium was electrically stimulated at the same location with a similar rate to that observed during the NE-induced arrhythmia. The total ventricular epicardial activation time for the pacing-induced arrhythmia increased from 21 ms (control, not shown) to 54 ms, and the activation maps for the NE- and pacing-induced arrhythmias were qualitatively similar (see Fig. 8). In two subsequent experiments, epicardial activation times increased from 14 and 18 ms (control) to 39 and 51 ms for the NE-induced arrhythmias and to 39 and 46 ms for the pacing-induced arrhythmias. The corresponding decreases in MAP were 15, 36, and 28 mmHg, respectively, for the NE-induced arrhythmias and 16, 31, and 27 mmHg, respectively, for the pacing-induced arrhythmias. The morphologies of the lead II ECG QRS complex were similar during corresponding NE- and pacing-induced ventricular arrhythmias.

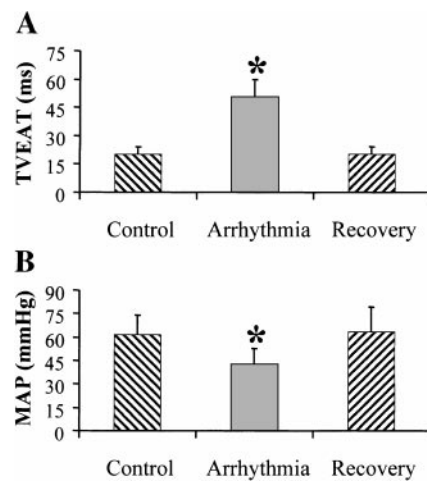


Fig. 7. Total ventricular epicardial activation time (TVEAT; A) and MAP (B) during control, ventricular arrhythmia, and recovery states for group B experiments ($n = 14$ animals, 29 observations). During the NE-induced ventricular arrhythmia, TVEAT significantly increased and MAP significantly decreased compared with control, $*P < 0.01$. The epicardial activation sequence and hemodynamics fully recovered after the NE infusion was stopped.

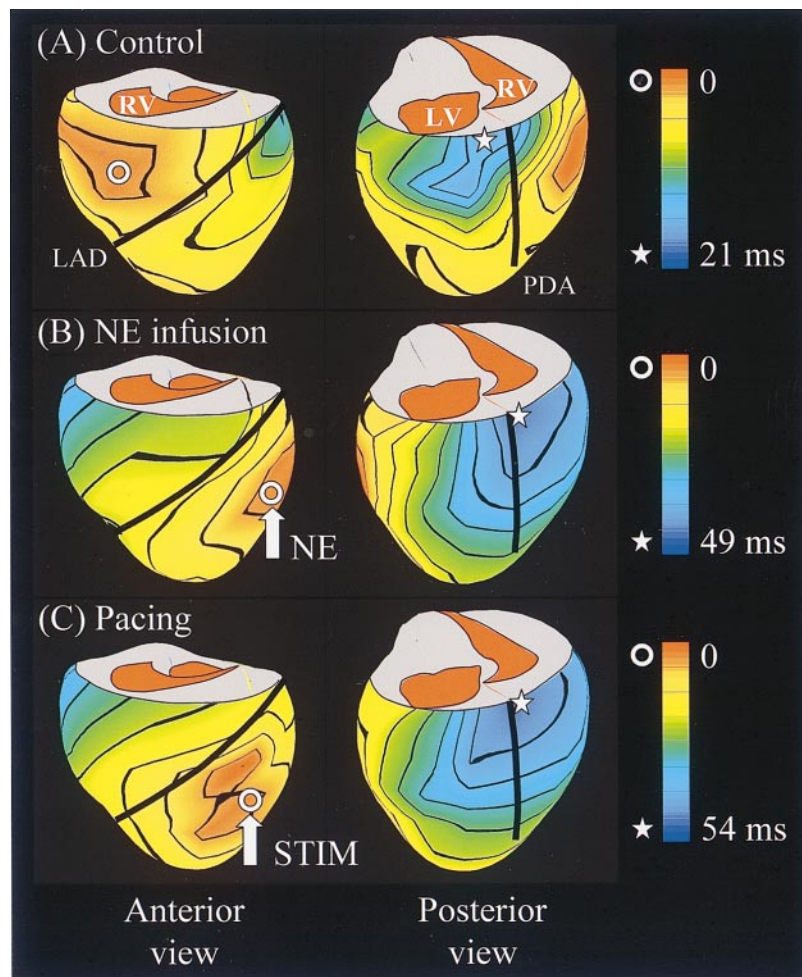


Fig. 8. Epicardial activation sequences during normal sinus rhythm (A) and ventricular arrhythmias induced chemically by subepicardial NE infusion (B) and electrically using epicardial electrical stimulation (STIM; C). Activation maps are superimposed on a 3D mathematical model of ventricular anatomy. During the ventricular arrhythmias, the location of earliest epicardial activation (o) shifted to the infusion/stimulation sites (thick white arrows), whereas latest epicardial activation (☆) remained in the posterobasal region. All events were fully reversible. Thick black lines represent the LAD and PDA coronary arteries.

Echocardiographic studies. Pacing-induced arrhythmias resulted in estimated ejection fraction decreases from 64, 52, and 50% (controls) to 20, 38, and 33%, respectively. Echocardiographic recordings were taken during two NE-induced arrhythmias, for which the estimated ejection fractions decreased from 60 and 55% (controls) to 30 and 30%, respectively. In all cases, mitral and aortic valve function remained normal.

Computer Modeling

At the beginning of the two-dimensional cellular network model simulation, the stimulated wave of electrical excitation proceeded “normally” from left to right, as illustrated in Fig. 9A. Several cycles later, the central region of NE-affected cells spontaneously depolarized before the normal wave of activation (Fig. 9B). A further seven cycles later, triggered automaticity was fully established, and the activation sequence was completely dominated by the central zone, which acted as an abnormal pacemaker with a rate of ~ 2 Hz (Fig. 9C). Spontaneous depolarization did not occur during the control simulation (not shown), for which calcium handling was unchanged.

Alternative simulations with 1) just the L-type calcium conductance increased and not the SR up-

take calcium conductance, 2) the L-type and SR uptake calcium conductances upregulated by a factor of two instead of five, and 3) the normal pacemaker reduced from 1 to 0.5 Hz also reproduced triggered automaticity, although the time to onset was greater in all three cases (simulation results not shown). The size of the NE-affected zone in the network model was varied to determine whether this altered arrhythmogenesis. NE-affected zones smaller than that described above did not result in arrhythmia, whereas larger zones did during the same simulated time period. Moreover, when the overall size of the network was increased (while the size of the central zone was kept constant), characteristics of the simulated arrhythmias remained unchanged, ruling out any mathematical edge effects on the required size of the NE-affected zone to elicit arrhythmia. To test whether other effects of NE could produce triggered automaticity, an alternative model simulation that incorporated modulation of the slow component of the delayed rectifier current and the sodium/potassium exchanger current instead of the calcium conductances was also performed (not shown). This model did not result in arrhythmia over the same simulated time period.

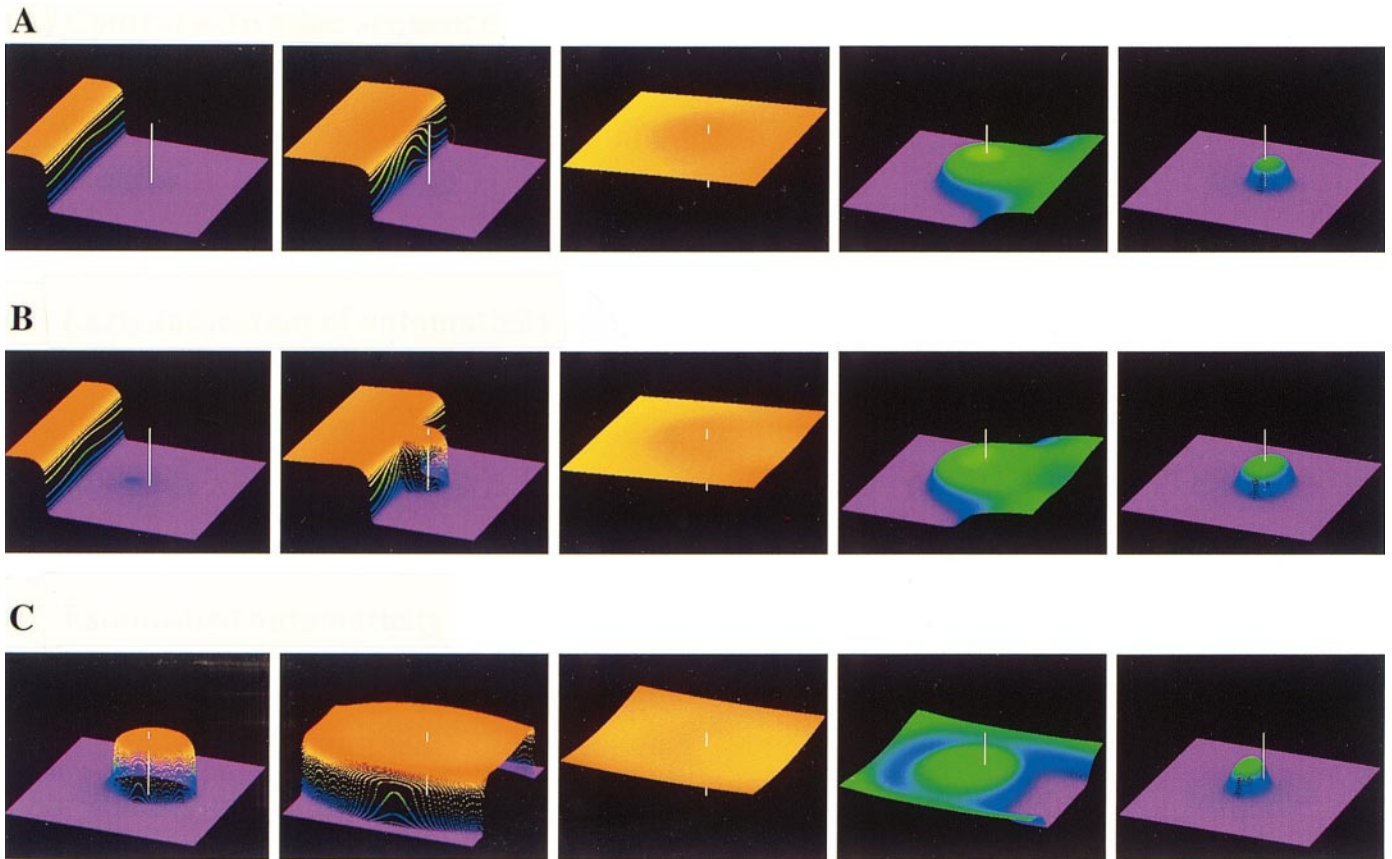


Fig. 9. Simulation of the activation sequence using a 2D mathematical model of ventricular myocardium for which the central region had high-adrenergic tone. Cellular transmembrane ionic currents described by a recent model (15) were incorporated into an arrangement of 256×256 resistively coupled myocytes. The L-type calcium-channel conductance and the sarcoplasmic reticulum (SR) calcium-ATPase uptake conductance were elevated by a factor of 5 at the center of the tissue sheet (white vertical marker). *A*: the control spread of activation proceeded from *left* to *right*, where red and indigo represent regions of depolarized and repolarized tissue, respectively. The central cells were last to repolarize, because the plateau phase of their action potentials was extended because of the upregulated calcium currents. *B*: triggered automaticity became apparent several cycles later, when the central region spontaneously depolarized just before the arrival of the control activation sequence. *C*: a further 7 cycles later, the central tissue was the dominant pacemaker and completely captured the activation sequence. The full animation may be viewed at the following internet address: <http://www.physiol.ox.ac.uk/~djp/NEarrhythmia/2Dnetsim.mpg>.

Analysis of the ionic behavior for a single-model cell with upregulated calcium conductances revealed a significant increase in the peak cytosolic calcium concentration and SR calcium release flux compared with the control case, as illustrated in Fig. 10. This led to spontaneous calcium release from the SR, which caused the sodium-calcium exchanger to admit sodium in an attempt to remove the excess calcium. The effect of this inward sodium current was to depolarize the cell beyond threshold. Spontaneous beating was sustained as long as intracellular calcium remained high.

DISCUSSION

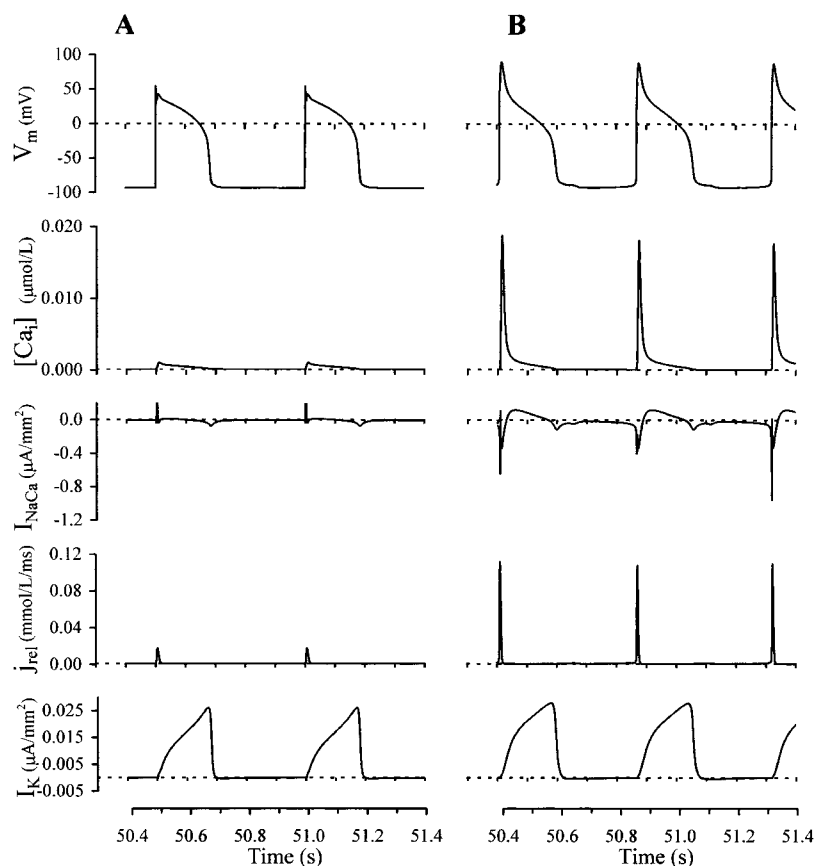
The new findings of this work are as follows. 1) Characterization of the epicardial electrical events during a ventricular arrhythmia, induced by a unifocal infusion of NE directly into the subepicardium, revealed activation patterns consistent with a region of triggered automaticity near the infusion site, which

could be comprehensively mimicked by epicardial pacing. 2) Stimulation of the right cardiac sympathetic or left or right cardiac vagal nerves abolished the NE-induced ventricular arrhythmia. 3) Two-dimensional computational reconstruction of the NE-induced arrhythmia replicated triggered automaticity due to calcium overload, which caused the sodium-calcium exchanger to act as an abnormal pacemaker.

Electromechanical Characterization of the NE-induced Ventricular Arrhythmia

We elicited a stable ventricular arrhythmia through subepicardial infusion of NE or by using epicardial electrical stimulation and compared the observed epicardial activation sequence with that obtained during control conditions. The location of NE infusion was randomly chosen throughout the exposed ventricles. During all sustained NE-induced arrhythmias, the zone of earliest ventricular epicardial activation con-

Fig. 10. A recent computational model (15) was used to quantify the changes in ventricular transmembrane potential (V_m) and ionic behavior between the control state, for which the model cell was continuously paced at 2 Hz with a twice-threshold stimulus for 2 ms (A), and under high-adrenergic tone (simulated by a 5-fold elevation of the L-type calcium-channel and SR calcium-ATPase uptake conductances; B), while paced as above for 50 s, after which time the stimulus was switched off and the cell exhibited automaticity. Up-regulating these conductances caused the peak cytosolic calcium concentration ($[Ca]_i$) and SR calcium release flux (j_{rel}) to increase markedly, compared with the control state, whereas the potassium current ($I_K = I_{Kr1} + I_{Kr2} + I_{Ks}$, where I_{Kr1} and I_{Kr2} are the rapid components and I_{Ks} is the slow component) remained similar. This intracellular calcium overload caused the sodium-calcium exchanger current (I_{NaCa}) to reverse and depolarize the cell, thus acting as an abnormal pacemaker with a spontaneous rate of ~ 2.2 Hz.



sistently matched the NE infusion site, and there was a significant increase in the total ventricular epicardial activation time compared with the control state. This was associated with a drop in cardiac output and ABP. Epicardial electrical stimulation near NE infusion sites that had previously been used to elicit ventricular arrhythmias closely mimicked the electrical events and hemodynamic changes associated with the NE-induced arrhythmias. Epicardial activation sequences and times were similar for the NE- vs. pacing-induced arrhythmias, as were the decreases in ABP, LVP, LVdP/dt, and LV ejection fraction, consistent with the notion that the region of tissue adjacent to the infusion site became the dominant pacemaker.

We chose a high concentration of NE ($10 \mu\text{mol/l}$ in saline at $150 \mu\text{l/min}$) because it elicited an arrhythmia within 1–5 min from the start of the infusion. Podzuweit et al. (18, 19) used the same concentration of NE in normal Tyrode infused at $10\text{--}20 \mu\text{l/min}$ and established arrhythmias within 2 min. They also reported arrhythmias with $1 \mu\text{mol/l}$ NE. We could not elicit reproducible arrhythmias using the reduced infusion rate, and this was most likely due to the absence of calcium in our infusate. To determine the effective region of influence of NE on the ventricular myocardium, Podzuweit (18) measured levels of cAMP in small ventricular tissue cores ($\sim 4\text{-mm}$ diameter and 6-mm length) at the onset of the arrhythmias and found that myocardial cAMP was $\sim 45\%$ greater in the 4-mm core at the infusion site compared with the

adjacent control tissue cores. The localized inhomogeneous nature of the NE infusion was critical in eliciting this arrhythmia because similar concentrations administered intravenously did not elicit the sustained ventricular arrhythmia. Furthermore, reversal of the arrhythmia by intravenous NE administration ($1 \mu\text{g}\cdot\text{kg}^{-1}\cdot\text{min}^{-1}$) is most likely due to the overdrive pacing effect of the sinoatrial node. This illustrates the requirement for localization of the effects of NE to the ventricular myocardium to elicit the sustained ventricular arrhythmia. The subepicardial infusion of NE was unlikely to have permanently damaged the affected cells, because the arrhythmia was fully reversible and could be elicited by using the same needle site on successive occasions with an interim period of full recovery of the activation sequence and hemodynamics.

Modulation of the NE-induced Ventricular Arrhythmia

The arrhythmia was also reproduced by subepicardial infusion of the specific β -agonist isoproterenol but not the α -agonist phenylephrine, whereas intravenous infusion of propranolol abolished the ectopic activity, consistent with a role for modulation of cAMP and calcium currents in arrhythmogenesis. Indeed, Podzuweit (18) elicited similar ventricular arrhythmias in the pig using intramyocardial infusion of a membrane-permeable analog of cAMP, inhibitors of cyclic nucleo-

tide phosphodiesterases, or NE. In that study, the NE-induced ectopic activity was abolished by the coinfusion of choline esters or calcium antagonists, but not by tetrodotoxin. These observations strongly implicate a β -adrenergic, cAMP modulation of intracellular calcium that leads to spontaneous depolarization of the ventricular myocardium. Catecholamines are known to enhance automaticity in Purkinje fibers (17), although this is not a unique property of specialized conducting fibers, because automaticity can also occur in isolated, perfused ventricular tissue (7). Moreover, catecholamines can induce afterdepolarizations in normal canine ventricular myocytes (21) and reentry in the ventricle (9). Therefore, we cannot exclude the possibility that spontaneous discharge may have elicited a premature stimulus to initiate ventricular reentry, although our results showed a regular cycle length and stationary site of earliest epicardial activation during the NE-induced arrhythmias.

The results of the present study show that stimulation of the right cardiac sympathetic nerves and intravenous infusion of NE can abolish the adrenergic-induced ventricular arrhythmia. Both interventions increased HR and facilitated the reestablishment of the sinoatrial node as the dominant pacemaker. Left- and right-sided vagal stimulation also abolished the arrhythmia (see the ECG trace in Fig. 4); however, ABP did not fully recover because of the decrease in HR caused by vagal stimulation itself. Vagal stimulation took ~ 7 s to terminate the arrhythmia, which is more characteristic of responses involving the indirect modulation of ion channels by intracellular messengers rather than the rapid activation of the acetylcholine-stimulated outward potassium current that can decrease HR within one or two heartbeats (4). The indirect effect of cholinergic activation, which is known to cause a decrease in the L-type calcium current in ventricular cells via the inhibition of adenylate cyclase-cAMP system (5) and via the nitric oxide-cGMP pathway (3, 25), is implicated in the antiarrhythmic property of vagal stimulation. Therefore, the antiarrhythmic effects of sympathetic and vagal nerve stimulation may act via two different mechanisms: the former directly restoring the natural site of pacemaking, and the latter involving a reduction in calcium currents and diastolic intracellular calcium in the ventricle.

Computational Reconstruction of the NE-induced Arrhythmia

Abnormal modulation of intracellular calcium is thought to be central to the NE-induced arrhythmia. First, the arrhythmia is abolished by β -adrenergic blockers (Ref. 18, see also RESULTS), calcium-channel antagonists, and choline esters (18). Second, it is initiated by permeant cAMP analogs (18). Therefore, we attempted to mimic aspects of this arrhythmia by altering calcium handling in a two-dimensional computational network of excitable cardiac myocytes. These changes led to intracellular calcium overload, which in

turn caused an abnormal influx of sodium through the sodium-calcium exchanger. This inward current depolarized the model cells beyond threshold and acted as an abnormal pacemaker (8). This suggests a possible cellular mechanism for the focal automaticity observed during subepicardial NE infusion.

Study Limitations

The preparation used for the present study was an open-chest, anesthetized pig. This altered the global ECG and could, therefore, have affected the magnitudes of the recorded epicardial electropotentials compared with the closed-chest animal. However, we recently found that the pattern of epicardial activation was not significantly altered after the chest had been reclosed (unpublished observation).

Perhaps the biggest limitation of this study is that the activation sequence was deduced from just epicardial electropotential recordings. For this reason, we cannot identify which specific cell types are responsible for the abnormal pacemaking during the NE infusion. Indeed, intracellular iontophoresis of cAMP enhances phase 4 depolarization and increases the rate of contraction in spontaneously active Purkinje fibers (24). In addition, the pig heart is known to host Purkinje tissue throughout the ventricular wall (23). Therefore, it is possible that the NE infusion enhanced Purkinje cell automaticity to elicit the arrhythmia. However, this is unlikely in the present preparation, because Purkinje fiber abnormal automaticity is unaffected by calcium-channel antagonism (8), whereas triggered automaticity is terminated by verapamil (8, 18, 27). Endocardial-to-epicardial ventricular cell heterogeneity may also play a role in the genesis of this arrhythmia, although this is difficult to determine because the electrophysiology of the various ventricular cell types in the pig is not well characterized.

Whereas our computational reconstruction implicates abnormal calcium handling in the central zone of the cellular network model, it is possible that automaticity could have arisen from a time-dependent decay of the potassium current (17), which has been shown to be modulated by catecholamines (2), coupled with a progressive activation of the L-type calcium-channel current. However, model simulations that incorporated modulation of the slow component of delayed rectifier current and the sodium/potassium exchanger current instead of the calcium conductances showed comparatively smaller effects. Other limitations of the computational model that prevent a direct comparison between the simulation results and in vivo measurements include species differences (guinea pig computational model vs. in vivo pig), topography (2-dimensional cellular network model vs. 3-dimensional in vivo ventricles), and effects of anisotropy (isotropic intercellular resistances vs. anisotropic in vivo conductances). Nevertheless, the computational model demonstrates that triggered automaticity can be reproduced by considering a small region of calcium-overloaded ventricular tissue.

The clinical correlates of this arrhythmia remain to be determined, although pathological circumstances can lead to high-sympathetic drive to a localized region of myocardium (10, 11, 16). We conclude that the ventricular arrhythmia described in this study is a likely consequence of spatial inhomogeneities in the concentration of NE in the ventricular myocardium that lead to triggered automaticity and result in depressed hemodynamics. Interventions that reestablish the sinoatrial node as the dominant pacemaker or that reduce regional inhomogeneities in NE may prevent or terminate this type of arrhythmia.

We thank Chris Hirst and Vivienne Harris for technical assistance and Dr. A. Banning for performing the echocardiography.

This study was supported by British Heart Foundation Programme Grant BG 95003. Computational simulations were made possible by support from the Oxford Supercomputing Centre of Oxford University and the Wellcome Trust, which provided access to two Silicon Graphics high-performance parallel computers.

REFERENCES

1. **Bean BB.** β -Adrenergic modulation of cardiac calcium channel gating. In: *Ion Channels in the Cardiovascular System: Function and Dysfunction*, edited by Spooner PM and Brown AM. Armonk, NY: Futura, 1994, p. 237–252.
2. **Giles W, Nakajima T, Ono K, and Shibata EF.** Modulation of the delayed rectifier K^+ current by isoprenaline in bull-frog atrial myocytes. *J Physiol (Lond)* 415: 233–249, 1989.
3. **Han X, Kobzik L, Zhao YY, Opel DJ, Liu WD, Kelly RA, and Smith TW.** Nitric oxide regulation of atrioventricular node excitability. *Can J Cardiol* 13: 1191–1201, 1997.
4. **Hartzell HC.** Regulation of cardiac ion channels by catecholamines, acetylcholine and second messenger systems. *Prog Biophys Mol Biol* 52: 165–247, 1988.
5. **Hescheler J, Kameyama M, and Trautwein W.** On the mechanism of muscarinic inhibition of the cardiac Ca^{2+} current. *Pflügers Arch* 407: 182–189, 1986.
6. **Hunter PJ, Smaill BH, Nielsen PMF, and Le Grice IJ.** A mathematical model of cardiac anatomy. In: *Computational Biology of the Heart*, edited by Panfilov AV and Holden AV. West Sussex, UK: Wiley, 1997, p. 171–215.
7. **Imanishi S and Surawicz B.** Automatic activity in depolarized guinea pig ventricular myocardium. Characteristics and mechanisms. *Circ Res* 39: 751–759, 1976.
8. **Lerman BB.** Response of nonreentrant catecholamine-mediated ventricular tachycardia to endogenous adenosine and acetylcholine. Evidence for myocardial receptor-mediated effects. *Circulation* 87: 382–390, 1993.
9. **Lerman BB, Stein KM, Markowitz SM, Mittal S, and Slotwiner D.** Catecholamine facilitated reentrant ventricular tachycardia: uncoupling of adenosine's antiadrenergic effects. *J Cardiovasc Electrophysiol* 10: 17–26, 1999.
10. **Mandel WJ.** Sustained monomorphic ventricular tachycardia. In: *Cardiac Arrhythmia: Mechanisms, Diagnosis, and Management*, edited by Podrid PJ and Kowey PR. London: Williams & Wilkins, 1995, p. 919–935.
11. **Mertes PM, el Abbassi K, Jaboin Y, Michel C, Beck B, Pinelli G, Carteaux JP, Villemot JP, and Burlet C.** Consequences of coronary occlusion on changes in regional interstitial myocardial neuropeptide Y and norepinephrine concentrations. *J Mol Cell Cardiol* 28: 1995–2004, 1996.
12. **Nash MP, Thornton JM, Banning AP, and Paterson DJ.** 3D epicardial activation sequence during a ventricular arrhythmia in the anesthetized pig (Abstract). *J Physiol (Lond)* 513.P: 162P, 1998.
13. **Nash MP, Thornton JM, and Paterson DJ.** Characterization of the epicardial electrical activation sequence during a ventricular arrhythmia in the anesthetized pig (Abstract). *J Physiol (Lond)* 507.P: 60P, 1998.
14. **Nielsen PM, Le Grice IJ, Smaill BH, and Hunter PJ.** Mathematical model of geometry and fibrous structure of the heart. *Am J Physiol Heart Circ Physiol* 260: H1365–H1378, 1991.
15. **Noble D, Varghese A, Kohl P, and Noble P.** Improved guinea-pig ventricular cell model incorporating a diadic space, I_{Kr} and I_{Ks} , and length- and tension-dependent processes. *Can J Cardiol* 14: 123–134, 1998.
16. **Palileo EV, Ashley WW, Swiryn S, Bauernfeind RA, Strassberg B, Petropoulos AT, and Rosen KM.** Exercise provokable right ventricular outflow tract tachycardia. *Am Heart J* 104: 185–193, 1982.
17. **Pappano AJ and Carmeliet EE.** Epinephrine and the pace-making mechanism at plateau potentials in sheep cardiac Purkinje fibers. *Pflügers Arch* 382: 17–26, 1979.
18. **Podzuweit T.** Catecholamine-cyclic-AMP- Ca^{2+} -induced ventricular tachycardia in the intact pig heart. *Basic Res Cardiol* 75: 772–779, 1980.
19. **Podzuweit T, Binz KH, Nennstiel P, and Flaig W.** The anti-arrhythmic effects of myocardial ischaemia. Relation to reperfusion arrhythmias? *Cardiovasc Res* 23: 81–90, 1989.
20. **Raisz E.** *Principles of Cartography*. New York: McGraw-Hill, 1962.
21. **Sosunov EA, Anyukhovskiy EP, Shvilkin A, Hara M, Steinberg SF, Danilo P Jr, Rosen MR, Moise NS, Merot J, Probst V, Charpentier F, Legeay Y, and Le Marec H.** Abnormal cardiac repolarization and impulse initiation in German shepherd dogs with inherited ventricular arrhythmias and sudden death. *Cardiovasc Res* 42: 65–79, 1999.
22. **Tomaselli GF and Marban E.** Electrophysiological remodeling in hypertrophy and heart failure. *Cardiovasc Res* 42: 270–283, 1999.
23. **Tranum-Jensen J, Wilde AAM, Vermeulen JT, and Jansen MJ.** Morphology of electrophysiologically identified junctions between Purkinje fibers and ventricular muscle in rabbit and pig hearts. *Circ Res* 69: 429–437, 1991.
24. **Tsien RW.** Adrenaline-like effects of intracellular iontophoresis of cyclic AMP in cardiac Purkinje fibres. *Nat New Biol* 245: 120–122, 1973.
25. **Wahler GM and Dollinger SJ.** Nitric oxide donor SIN-1 inhibits mammalian cardiac calcium current through cGMP-dependent protein kinase. *Am J Physiol Cell Physiol* 268: C45–C54, 1995.
26. **Winslow RL, Varghese A, Noble D, Adlakha C, and Hoythya A.** Generation and propagation of ectopic beats induced by spatially localized Na-K pump inhibition in atrial network models. *Proc R Soc Lond B Biol Sci* 254: 55–61, 1993.
27. **Wit AL and Cranefield PF.** Triggered and automatic activity in the canine coronary sinus. *Circ Res* 41: 434–445, 1977.